Original Article

Sensitivity and specificity of amide proton transfer-weighted imaging for assessing programmed death-ligand 1 status in non-small cell lung cancer: a comparative study with intravoxel incoherent motion and ^{18}F-FDG PET

Nan Meng[1,2#], Fangfang Fu[1#], Jing Sun[3#], Pengyang Feng[4], Yu Luo[1], Yaping Wu[1], Xiaochen Li[1], Jianmin Yuan[5], Yang Yang[6], Hui Liu[7], Zhe Wang[5], Meiyun Wang[1,2]

[1]Department of Medical Imaging, Zhengzhou University People's Hospital & Henan Provincial People's Hospital, Zhengzhou, China; [2]Academy of Medical Sciences, Zhengzhou University, Zhengzhou, China; [3]Department of Pediatrics, Zhengzhou Central Hospital, Zhengzhou University, Zhengzhou, China; [4]Department of Medical Imaging, Henan University People's Hospital & Henan Provincial People's Hospital, Zhengzhou, China; [5]Central Research Institute, United Imaging Healthcare Group, Shanghai, China; [6]Beijing United Imaging Research Institute of Intelligent Imaging, United Imaging Healthcare Group, Beijing, China; [7]United Imaging Healthcare America, Inc., Houston, TX, USA

Contributions: (I) Conception and design: M Wang, N Meng; (II) Administrative support: M Wang, F Fu; (III) Provision of study materials or patients: N Meng, P Feng, Y Luo; (IV) Collection and assembly of data: J Sun, X Li, Y Wu; (V) Data analysis and interpretation: J Yuan, Y Yang, H Liu, Z Wang; (VI) Manuscript writing: All authors; (VII) Final approval of manuscript: All authors.

[#]These authors contributed equally to this work and should be considered as co-first authors.

Correspondence to: Meiyun Wang. Department of Medical Imaging, Zhengzhou University People's Hospital & Henan Provincial People's Hospital, 7 Weiwu Road, Zhengzhou 450000, Henan, China. Email: mywang@zzu.edu.cn.

Background: Noninvasive assessment of programmed death-ligand 1 (PD-L1) expression status in non-small cell lung cancer (NSCLC) is necessary. This study arm to investigate the value of 2-[^{18}F]-fluoro-2-deoxy-D-glucose positron emission tomography (^{18}F-FDG PET), diffusion-weighted imaging (DWI), intravoxel incoherent motion (IVIM), and amide proton transfer-weighted imaging (APTWI) in the assessment of PD-L1 status in NSCLC.

Methods: This is a prospective diagnostic study. A total of 76 patients with NSCLC underwent chest ^{18}F-FDG PET/magnetic resonance imaging (MRI). Parameters maximum standardized uptake value (SUV_{max}), quantitate the metabolic tumor volume (MTV), total lesion glycolysis (TLG), apparent diffusion coefficient (ADC), diffusion coefficient (D), pseudo diffusion coefficient (D*), and perfusion fraction (f), and magnetization transfer ratio asymmetry at 3.5 ppm [MTRasym (3.5 ppm)] from ^{18}F-FDG PET, DWI, IVIM, and APTWI, respectively, were compared. The optimal combination of parameters was investigated using logistic regression models and evaluated by area under the receiver operating characteristic (ROC) curve (AUC). The bootstrap with 1,000 samples was used for model validation.

Results: SUV_{max}, MTV, TLG, and MTRasym (3.5 ppm) were higher and D and f were lower in PD-L1 positive NSCLC than in PD-L1 negative NSCLC (all $P<0.05$). Logistic analysis showed that the combination of MTRasym (3.5 ppm), D, and SUV_{max} had the strongest predictive value for the differentiation of PD-L1 positive and PD-L1 negative NSCLC [AUC, 0.946; 95% confidence interval (CI): 0.869–0.985; sensitivity, 85.29%; specificity, 91.67%; P all <0.001]. The verification model showed the combination of MTRasym (3.5 ppm), D, and SUV_{max} had the strongest predictive value, and its ROC curve and calibration curve showed good accuracy (AUC, 0.919, 95% CI: 0.891–0.937) and consistency.

Conclusions: Multi-parametric ^{18}F-FDG PET/MRI is beneficial for the non-invasive assessment of PD-L1 status in NSCLC patients, and the combination of SUV_{max}, D, and MTRasym (3.5 ppm) may serve as a

prognostic biomarker to guide immunotherapy.

Keywords: Non-small cell lung cancer (NSCLC); programmed death-ligand 1 (PD-L1); amide proton transfer-weighted imaging (APTWI); intravoxel incoherent motion (IVIM); positron emission tomography (PET)

Submitted Feb 25, 2022. Accepted for publication Jun 07, 2022.
doi: 10.21037/qims-22-189
View this article at: https://dx.doi.org/10.21037/qims-22-189

Introduction

Non-small cell lung cancer (NSCLC) accounts for approximately 85% of all lung cancer cases, has a five-year survival rate of only 15%, and is considered the leading cause of cancer-related deaths globally (1,2). Programmed death-ligand 1 (PD-L1) is a transmembrane protein, and its engagement with programmed cell death protein 1 (PD-1) represents an essential immune checkpoint that has been proven to manipulate the immune response against cancer (3). Recent studies have shown that PD-L1 inhibitors exhibit a survival benefit compared to conventional standard therapy in patients with NSCLC (4-6). Currently, immunohistochemistry is a common method used for the clinical measurement of PD-L1; however, this procedure requires biopsied or surgical tissue specimens, which are correlated with the risk of morbidities and collected by invasive procedures (7). Therefore, it is important to find an alternative noninvasive method to measure PD-L1 status, especially in cases where immunohistochemistry has failed or no tissue is available (8).

2-[^{18}F]-fluoro-2-deoxy-D-glucose positron emission tomography/computed tomography (^{18}F-FDG PET/CT) has the ability to serve as a valuable predictive biomarker for the detection of genetic mutations (9). Several researchers have found a positive association between the maximum standardized uptake value (SUV_{max}) and PD-L1 expression in NSCLC (10,11). However, considering the inadequacy of CT in terms of reflecting only the morphological features of lesions, it is difficult for ^{18}F-PET/CT to reflect the microscopic features of lesions from a perspective other than metabolic information. PET/magnetic resonance imaging (MRI) allows multimodal quantitative MRI sequences to be scanned in parallel with PET imaging, providing a more multidimensional reflection of lesion information. Diffusion-weighted imaging (DWI) is an MRI imaging sequence that can reflect the diffusion movement of water molecules in tissues (12). Previous studies have shown that the apparent diffusion coefficient (ADC), a quantitative parameter of DWI, was negatively correlated with PD-L1 expression in head and neck squamous cell carcinomas to some extent (13,14). Intravoxel incoherent motion (IVIM) is an extension of conventional DWI that can obtain both the water molecule diffusion and microperfusion information of a lesion in a single scan due to the introduction of multiple b-values (15). Amide proton transfer-weighted imaging (APTWI), known as the indigent version of molecular imaging, is a magnetic resonance (MR) imaging technology proposed by Zhou *et al.* that is based on the chemical exchange between amide protons and water protons and can achieve the noninvasive quantitative assessment of mobile protein and peptide concentrations in tissues without the use of contrast agents (16). Currently, although a small number of studies have separately explored the value of IVIM or APTWI in the noninvasive assessment of subtypes, cell proliferation, or epidermal growth factor receptor (EGFR) expression in lung cancer (17-20), to our knowledge, no report has applied IVIM or APTWI in the evaluation of PD-L1 expression status in NSCLC.

In the present study, we aimed to investigate the contributory value of ^{18}F-FDG PET, DWI, IVIM, and APTWI-related parameters for the noninvasive prediction of PD-L1 expression status in NSCLC, offering an optional reference for the clinical management of these patients. We present the following article in accordance with the STARD reporting checklist (available at https://qims.amegroups.com/article/view/10.21037/qims-22-189/rc).

Methods

Study participants

The study was conducted in accordance with the Declaration of Helsinki (as revised in 2013). This prospective study was complied with ethical committee standards and approved by the ethics committee of

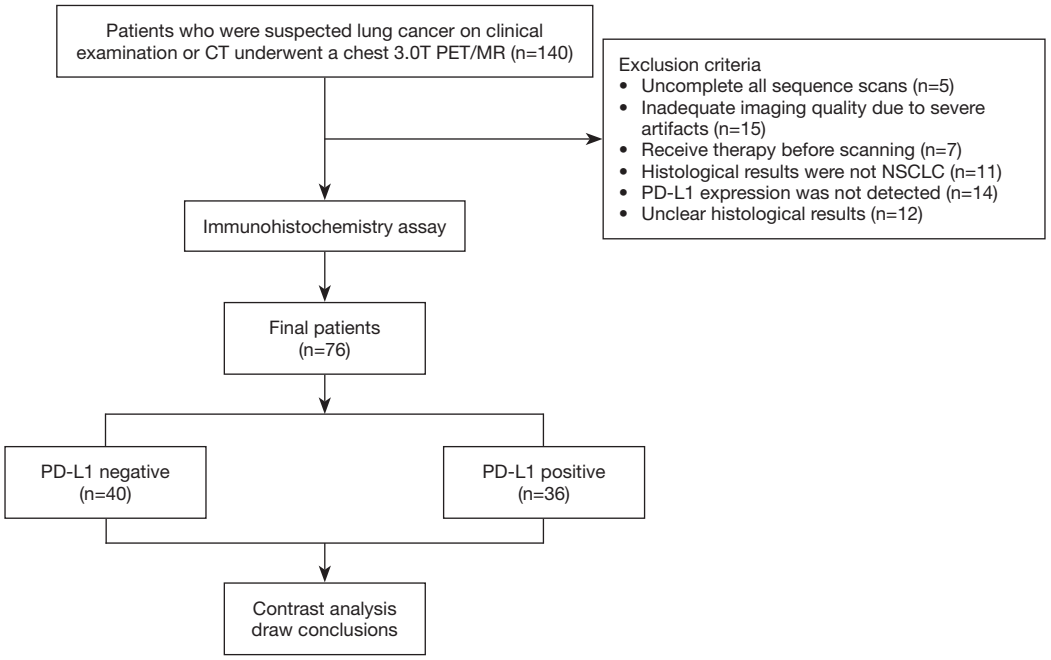

Figure 1 Flow diagram of the patient selection process. CT, computed tomography; PET, positron emission tomography; MR, magnetic resonance; NSCLC, non-small cell lung cancer; PD-L1, programmed death-ligand 1.

the Zhengzhou University People's Hospital & Henan Provincial People's Hospital (No. 2018067) and informed consent was taken from all individual participants. From December 2020 to January 2022, a series of 140 patients underwent chest multiparametric ^{18}F-FDG PET/MRI due to suspected lung cancer on clinical examination or CT. The following patients were excluded: (I) patients with claustrophobia or other diseases that prevent them from completing all the sequences (n=5); (II) patients with inadequate DWI, IVIM or APTWI imaging quality for analysis due to severe artifacts (n=15); (III) participants who have received relevant treatment prior to scanning (n=7); (IV) patients with histological results that were not NSCLC (n=11); (V) patients who were not tested for PD-L1 expression (n=14); and (VI) patients with unclear histological results (n=12). Ultimately, 76 patients were enrolled in the present study (*Figure 1*).

Image acquisition

A hybrid 3.0 T PET/MR system (uPMR 790, UIH, Shanghai, China) with a 12-channel phased-array body coil was used in this study. All patients were placed in the supine position with the head first and were scanned from the upper thoracic inlet to the lower lung margin, and a breathing strap was attached to the patient's abdomen to monitor breathing. ^{18}F-FDG was obtained by FracerLab FX-FDG (GE Minitrac, Chicago , USA) and had a pH of 4.5–8.5 and purity of >95%. All patients fasted for a minimum of 6 hours prior to the scan to ensure that their serum glucose levels were <6.5 mmol/L when injecting ^{18}F-FDG (0.11 mCi/kg). The scan was initiated 60 minutes after injection of ^{18}F-FDG. A 3D T1-weighted spoiled gradient-echo sequence with Dixon-based water-fat separation imaging (WFI) was used to do the MR-based attenuation correction (MRAC). During the MRAC processing, the corrected images were segmented into four classes: soft tissue, fat, lung, and air (21,22). Four categories of soft tissue, fat, lung and air are segmented in the MRAC processing of the corrected images. The time of PET acquisition was 27 min, and OSEM was used to reconstruct the PET images. The PET is reconstructed according to the following parameters: voxel size =2.6×2.6×2.0 mm^3, number of iterations =2, subsets =20. In parallel with PET scanning, T1-weighted imaging (T1WI), T2-weighted imaging (T2WI), and DWI were performed first. Then, all slices containing lesions were selected from DWI images, and their positions, layer thickness, and layer spacing were copied to IVIM and APTWI for the corresponding scanning. *Table 1* showed details of the protocol.

Table 1 Imaging protocol parameters

Parameters	Wfi3d-trig	T1WI	T2WI	DWI	IVIM	APTWI
Sequence	2D-FSE	2D-FSE	2D-FSE	2D-SS-EPI	2D-SS-EPI	2D-FSE
Orientation	Axial	Axial	Axial	Axial	Axial	Axial
Repetition time/echo time (ms)	4.92/2.24	5.06/2.1	3,315/87.8	1,620/69.6	1,620/69.6	4,500/42.56
Field of view (cm^2)	35×50	35×50	35×50	35×50	35×50	35×50
Matrix	192×192	303×456	264×480	202×256	202×256	128×100
Bandwidth (Hz/pixel)	–	260	260	2,370	2,370	500
Slice thickness (mm)	2	5	5	5	5	5
Interval (mm)	0	1	1	1	1	1
Number of excitations	2	2	2	1, 8	1, 1, 2, 2, 4, 4, 6, 6, 8, 10	1
Fat suppression	No	No	Yes	Yes	Yes	No
b-values (s/mm^2)	–	–	–	0, 800	0, 25, 50, 100, 150, 200, 400, 600, 800, 1,000	–
Respiratory compensation	Yes	Yes	Yes	Yes	Yes	Yes
Scan time	2 min 04 s	14 s	2 min 26 s	2 min 58 s	3 min 38 s	3 min 15 s (single slice)

For APTWI: B_1 =1.3 μT and 2.5 μT, ETL =39, Gaussian pulse, 10 repeats, 100 ms duration, plus one S_0 with no CEST saturation pulse for normalization, Δ spanned from [–4.5, 4.5] ppm in 31 steps; 11 low power B_1 =0.13 μT, Δ spanned from [–1.0, 1.0] ppm images were collected as WASSAR images for B_0 map correction. Wfi3d-trig, 3D T1-weighted spoiled gradient-echo sequence with Dixon-based water-fat separation imaging; T1WI, T1-weighted imaging; T2WI, T2-weighted imaging; DWI, diffusion-weighted imaging; IVIM, intravoxel incoherent motion; APTWI, amide proton transfer-weighted imaging; FSE, fast spin echo; SS-EPI, single shot echo planar imaging.

Data generation

All Data were transferred to the UIH Workstation (uWS-MR: R005) and analyzed by two nuclear medicine physicians (NM and FF, with 6 and 15 years of experience), independently. The metabolic parameters were postprocessed using fused PET/MRI software, where the volume of interest (VOI) was automatically extracted and a 40% SUV_{max} was applied as a threshold to calculate the total lesion glycolysis (TLG), metabolic tumor volume (MTV), and SUV_{max} (23). Postprocessing of MRI parameters was performed with specialized software in the advanced analysis toolkit. The parameter of DWI was generated using the following equation:

$$S_b/S_0 = \exp(-b \times ADC) \quad [1]$$

where ADC is the apparent diffusion coefficient, b is the diffusion sensitizing factor, and S_0 and S_b are the signal intensities (SIs) under different b values (0 s/mm^2 and other values, respectively) (12). The IVIM parameters were drawn from the following formula:

$$S_b/S_0 = (1-f) \times \exp(-bD) + f \times \exp[-b \times (D^*+D)] \quad [2]$$

where D, D*, and f represent the true diffusion coefficient, pseudo diffusion coefficient, and perfusion fraction, respectively (15). The APTWI parameter was derived from the following equation:

$$MTRasym(3.5\ ppm) = [S_{sat}(-3.5\ ppm) - S_{sat}(+3.5\ ppm)]/S_0 \quad [3]$$

where the magnetization transfer ratio was defined as 1 – S_{sat}/S_0, MTRasym (3.5 ppm) was the magnetization transfer ratio asymmetry at 3.5 ppm downfield from the water signal, and S_{sat} and S_0 represent the SIs obtained with and without selective saturation, respectively (16). Referring to the PET/MR fusion image, the region of interest (ROI) was manually delineated layer by layer along the medial side of the tumor margin on each axial T2WI image with tumor, avoiding areas of obvious necrosis. The software automatically copies all ROIs to each parameter map to calculate the average values based on the gross tumour volume (GTV).

Table 2 Clinicopathologic characteristics of patients

Variables	PD-L1 negative (n=40)	PD-L1 positive (n=36)	P value
Age (years)	63.38±9.74	63.08±7.79	0.887
Maximum diameter (mm)	27.28±10.49	37.11±15.55	0.002*
Male, n (%)	18 (40.00)	24 (63.89)	0.058
Smoking, n (%)	19 (47.50)	17 (47.22)	0.981
TNM stage, n (%)			
IA2	6 (15.00)	2 (5.56)	0.180
IA3	5 (12.50)	1 (2.78)	0.117
IB	4 (10.00)	1 (2.78)	0.205
IIB	5 (12.50)	3 (8.33)	0.555
IIIA	0 (0.00)	3 (8.33)	0.062
IIIB	5 (12.50)	7 (19.44)	0.407
IIIC	0 (0.00)	3 (8.33)	0.062
IVA	6 (15.00)	5 (13.89)	0.891
IVB	9 (22.50)	11 (30.56)	0.426
Grade, n (%)			
I	8 (20.00)	16 (44.44)	0.022*
II	19 (47.50)	16 (44.44)	0.790
III	13 (32.50)	4 (11.12)	0.025*
Subtype, n (%)			
AC	29 (72.50)	21 (58.33)	0.194
SCC	11 (27.50)	15 (41.67)	0.194

*, indicates statistically significant differences. PD-L1, programmed cell death-ligand 1; TNM, tumor node metastasis classification; AC, adenocarcinoma; SCC, squamous cell carcinoma.

PD-L1 expression

All sections were stained with the Dako PD-L1 22C3 pharmDx kit (Monoclonal mouse anti-human antibody, Clone 22C3, Dako North America, Inc., Carpinteria, CA, USA) using the Dako Autostainer Link 48 Platform (Dako), and the specific protocol of immunohistochemical staining for PD-L1 expression was carried out as previously described procedures (24). The tumor proportion score (TPS), which is the percentage of viable tumor cells showing membrane PD-L1 staining relative to all live tumor cells, was used to assess the level of PD-L1 expression, where TPS ≥1% was defined as PD-L1 positive (8). All histopathology analyses were performed by two experienced pathologists (QY. L and DJ. L, with 5 and 10 years of experience) who were blinded to the imaging findings and clinical information, and in the case of a disagreement, the two pathologists had a mutual discussion to reach a consensus.

Statistical analysis

Statistical analyses were performed with MedCalc (Version 15.0; MedCalc Software, Ostend, Belgium), R (Version 3.5.3; R Foundation, Auckland, Zealand), and SPSS (Version 23.0; IBM, New York, USA) software, and $P<0.05$ was considered statistically significant. Interobserver agreement was assessed by the intraclass correlation coefficient (ICC), where $r\geq0.75$ was excellent agreement, $0.60\leq r<0.75$ was good agreement, $0.40\leq r<0.60$ was fair agreement, and $r<0.40$ was poor agreement (25). The Shapiro-Wilk test was applied to test the normality of the data, where normally distributed data (mean ± SD) were compared using the independent-sample *t*-test and non-normally distributed data (median and interquartile range) were compared using the Mann-Whitney U test. The area under the receiver operating characteristic (ROC) curve (AUC) was used to describe the diagnostic efficacy, and the differences were compared using the DeLong test. Parameters that were statistically significant ($P<0.1$) in the univariate logistic regression analysis were enrolled in the following multivariate analysis. Multivariate logistic regression models are used to determine the best combination of parameters. A control model was built by bootstrapping (1,000 samples), which we tested with multiple regressions and verified its performance with calibration curves, decision curve analysis (DCA), and ROC curves.

Results

Participants details

A total of 76 patients with 76 lesions were included in this study, including 42 males and 34 females, with a mean age of 64 years, ranging from 34 to 81 years, and with a mean lesion size of 14.14 cm^3, ranging from 1.77 to 229.85 cm^3. The details of participants are provided in *Table 2* and *Figure 2*, respectively.

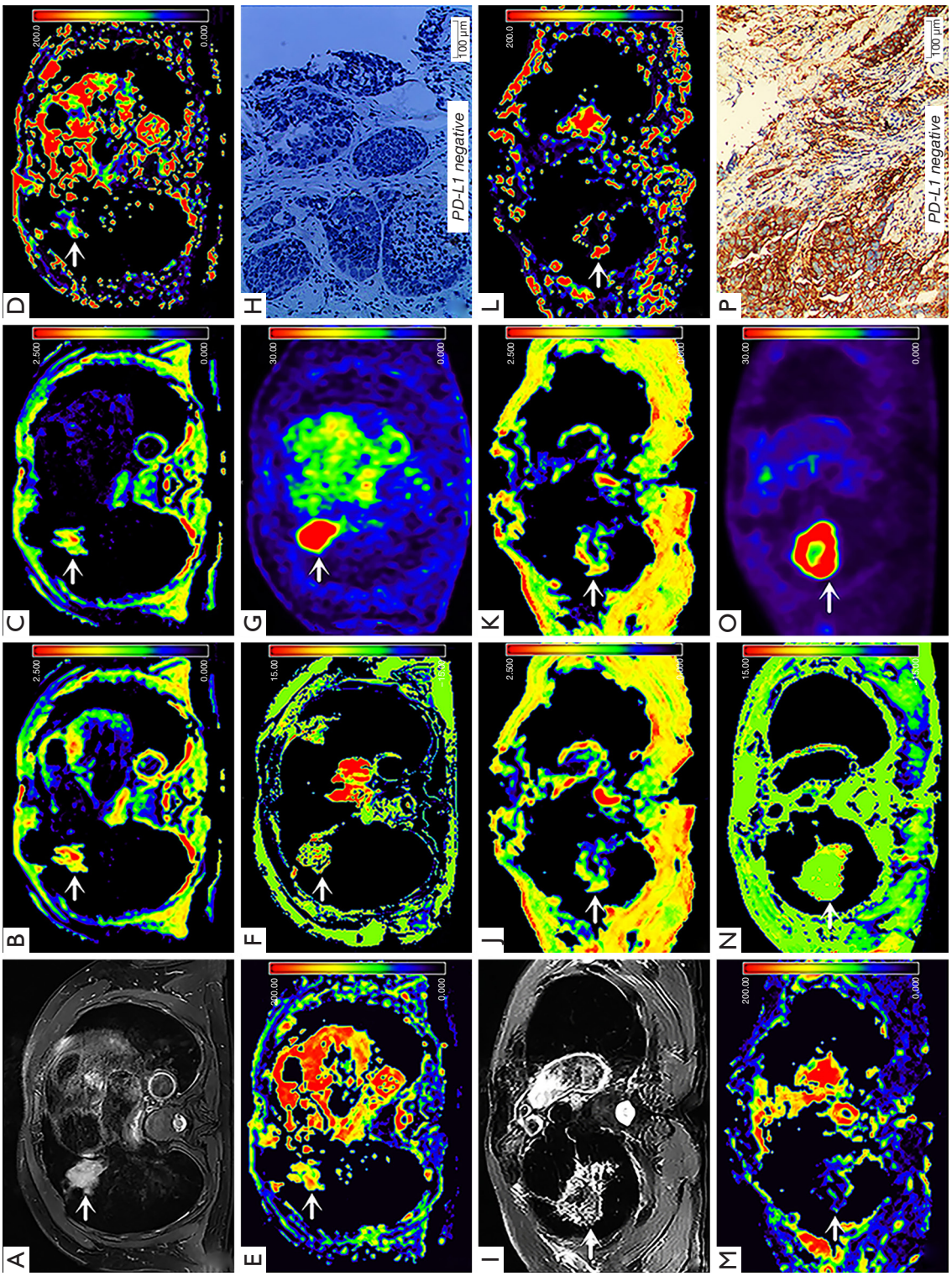

Figure 2 Multiparametric PET-MRI images and immunohistochemistry images of different patients. (A-H) A 74-year-old man with squamous cell carcinoma (white arrow, smoker, maximum diameter 36 mm, grade III, stage IVA, PD-L1 negative, and TPS =0%). (I-P) A 73-year-old man with adenocarcinoma (white arrow, smoker, maximum diameter 38 mm, grade III, stage IVA, PD-L1 positive, and TPS =95%). (A,I) Maps of T2WI; (B,J) pseudocolored maps of ADC; (C,K) pseudocolored maps of D; (D,L) pseudocolored maps of D*; (E,M) pseudocolored maps of f; (F,N) pseudocolored maps of MTRasym (3.5 ppm); (G,O) pseudocolored maps of ^{18}F-FDG PET; and (H,P) immunohistochemistry maps of PD-L1 expression (×200). PET-MRI, positron emission tomography/magnetic resonance imaging; PD-L1, programmed cell death-ligand; TPS, tumor proportion score; T2WI, T2-weighted imaging; ADC, apparent diffusion coefficient; D, diffusion coefficient; D*, pseudo diffusion coefficient; f, perfusion fraction; MTRasym (3.5 ppm), magnetization transfer ratio asymmetry at 3.5 ppm; ^{18}F-FDG, 2-[^{18}F]-fluoro-2-deoxy-D-glucose.

Table 3 Comparison of different parameters among different groups

Parameters	PD-L1 negative	PD-L1 positive	*t*/*z* value	P value
ADC ($\times10^{-3}$ mm^2/s)	1.32±0.31	1.34±0.22	−0.203	0.840[a]
D ($\times10^{-3}$ mm^2/s)	1.18±0.22	1.03±0.09	3.921	<0.001[a#]
D* ($\times10^{-3}$ mm^2/s)	26.82 (8.52, 55.91)	30.41 (15.52, 61.49)	−0.629	0.529[b]
f (%)	33.27 (23.12, 42.67)	24.11 (15.09, 33.98)	−2.497	0.013[b#]
MTRasym (3.5 ppm) (%)	2.08 (1.01, 2.95)	3.03 (2.00, 5.03)	−3.308	0.001[b#]
SUV_{max} (g/cm^3)	5.49 (3.79, 9.73)	11.64 (7.56, 17.98)	−4.505	<0.001[b#]
MTV (cm^3)	4.98 (1.90, 13.53)	18.02 (5.89, 34.31)	−3.610	<0.001[b#]
TLG (g)	11.74 (4.47, 59.87)	83.42 (40.81, 195.27)	−4.328	<0.001[b#]

Data are presented as mean ± SD or median (interquartile range). [a], independent *t*-test; [b], Mann-Whitney U test. [#], indicates the comparison with statistical significance. PD-L1, programmed cell death-ligand 1; ADC, apparent diffusion coefficient; D, diffusion coefficient; D*, pseudo diffusion coefficient; f, perfusion fraction; MTRasym (3.5 ppm), magnetization transfer ratio asymmetry at 3.5 ppm; SUV_{max}, maximum standardized uptake value; MTV, metabolic tumor volume; TLG, total lesion glycolysis.

Interobserver agreement

The ADC, D, D*, f, and MTRasym (3.5 ppm) measured by the 2 readers had an excellent interobserver agreement. The ICC were 0.918 (95% CI: 0.870–0.949), 0.892 (95% CI: 0.826–0.933), 0.841 (95% CI: 0.748–0.900), 0.894 (95% CI: 0.832–0.934), and 0.865 (95% CI: 0.786–0.915). Therefore, the 2 readers' mean results of above parameters were applied for analyses.

Comparison of different groups

MTRasym (3.5 ppm), SUV_{max}, MTV, and TLG were higher and D and f were lower in PD-L1-positive NSCLC than in PD-L1-negative NSCLC (all P<0.05), and there was no significant difference in ADC and D* between the two groups (P=0.840, 0.529). Detailed comparisons of different parameters are shown in *Table 3*.

Regression analyses

Sex, age, maximum diameter, smoking status, subtype, stage, grade, and derived parameters were all enrolled in regression analyses. Univariate analysis showed that sex, maximum diameter, stage, grade, ADC, D, f, MTRasym (3.5 ppm), SUV_{max}, MTV, and TLG were predictors (all P<0.1), and multivariate analysis showed that only SUV_{max}, D, and MTRasym (3.5 ppm) were independent predictors (P=0.016, 0.007, and 0.004, respectively) (*Table 4*).

Diagnostic efficiency

The ROC analysis showed that SUV_{max}, MTV, TLG, D, f, and MTRasym (3.5 ppm) all had a positive effect on predicting PD-L1 expression in NSCLC, and the AUCs were 0.801, 0.741, 0.789, 0.743, 0.667, and 0.766, respectively (all P<0.05). The combination of independent predictors [SUV_{max}, D, and MTRasym (3.5 ppm)] had the strongest predictive potential (AUC =0.946; sensitivity, 86.11%; specificity, 92.50%; P<0.001), and the differences between AUC [SUV_{max} + D + MTRasym (3.5 ppm)] and AUC (SUV_{max}), AUC (MTV), AUC (TLG), AUC (D), AUC (f), and AUC [MTRasym (3.5 ppm)] were all significant (Z=3.372, 3.293, 2.996, 3.688, 4.626, and 3.517, respectively; P=0.001, 0.001, 0.003, <0.001, <0.001, and <0.001 (*Table 5*, *Figure 3*).

Validation of model

In the control model based on bootstrapped samples, the combination of SUV_{max}, D, and MTRasym (3.5 ppm) also had the maximum predictive value. And in ROC analysis, the model had an AUC of 0.919 (95% CI: 0.891–0.937), the calibration curve indicated that the model had high consistency in predicting PD-L1 expression in NSCLC, and the DCA showed that the model could provide a high net benefit for relevant patients (*Figure 4*).

Discussion

As a nonspecific tracer, the uptake of ^{18}F-FDG in tissues

Table 4 Univariate and multivariate analyses

Parameters	Univariate analyses		Multivariate analyses	
	OR (95% CI)	P value	OR (95% CI)	P value
Age (year)	0.996 (0.946–1.049)	0.885	–	–
Sex	0.409 (0.161–1.039)	0.060	0.208 (0.021–2.094)	0.183
Smoking	1.955 (0.779–4.910)	0.153	–	–
Maximum diameter (mm)	1.799 (1.210–2.675)	0.004#	0.919 (0.344–2.455)	0.866
Subtype	2.143 (0.808–5.683)	0.126	–	–
Stage	1.186 (1.017–1.382)	0.029#	0.919 (0.658–1.283)	0.620
Grade	0.453 (0.233–0.880)	0.020#	1.701 (0.381–7.590)	0.486
ADC ($\times10^{-3}$ mm^2/s)	1.189 (0.222–6.376)	0.840	–	–
D ($\times10^{-3}$ mm^2/s)	0.256 (0.108–0.604)&	0.002#	0.081 (0.013–0.503)&	0.007#
D* ($\times10^{-3}$ mm^2/s)	1.002 (0.992–1.012)	0.727	–	–
f (%)	0.957 (0.922–0.993)	0.018#	0.997 (0.961–1.035)	0.894
MTRasym (3.5 ppm) (%)	2.080 (1.386–3.121)	<0.001#	4.550 (1.609–12.863)	0.004#
SUV_{max} (g/cm^3)	1.299 (1.136–1.486)	<0.001#	1.517 (1.079–2.133)	0.016#
MTV (cm^3)	1.096 (1.037–1.159)	0.001#	1.172 (0.953–1.442)	0.132
TLG (g)	1.018 (1.006–1.030)	0.002#	0.984 (0.951–1.019)	0.373

&, OR for per 1 standard deviation; #, indicates the logistic regression analyses with statistical significance. PD-L1, programmed cell death-ligand 1; OR, odds ratio; CI, confidence interval; ADC, apparent diffusion coefficient; D, diffusion coefficient; D*, pseudo diffusion coefficient; f, perfusion fraction; MTRasym (3.5 ppm), magnetization transfer ratio asymmetry at 3.5 ppm; SUV_{max}, maximum standardized uptake value; MTV, metabolic tumor volume; TLG, total lesion glycolysis.

Table 5 Predictive performance for identifying PD-L1 negative and positive NSCLC

Parameters	AUC (95% CI)	P value	Cutoff	Sensitivity, %	Specificity, %	Comparison with a combined diagnosis
ADC ($\times10^{-3}$ mm^2/s)	0.534 (0.416–0.649)	0.614	–	–	–	–
D ($\times10^{-3}$ mm^2/s)	0.743 (0.630–0.836)	<0.001#	1.140	97.22	50.00	Z=3.688, P<0.001#
D* ($\times10^{-3}$ mm^2/s)	0.542 (0.424–0.657)	0.530	–	–	–	–
f (%)	0.667 (0.549–0.771)	0.007#	36.24	88.89	42.50	Z=4.626, P<0.001#
MTRasym (3.5 ppm) (%)	0.766 (0.655–0.856)	<0.001#	3.570	47.22	95.00	Z=3.517, P<0.001#
SUV_{max} (g/cm^3)	0.801 (0.693–0.884)	<0.001#	5.900	88.89	60.00	Z=3.372, P=0.001#
MTV (cm^3)	0.741 (0.628–0.835)	<0.001#	16.57	55.56	92.50	Z=3.293, P=0.001#
TLG (g)	0.789 (0.680–0.874)	<0.001#	71.75	58.33	85.00	Z=2.996, P=0.003#
Combined diagnosis	0.946 (0.869–0.985)	<0.001#	–	86.11	92.50	–

The combined diagnosis represents MTRasym (3.5 ppm) + D + SUVmax. #, indicates statistically significant differences. PD-L1, programmed cell death-ligand 1; NSCLC, non-small cell lung cancer; ADC, apparent diffusion coefficient; D, diffusion coefficient; D*, pseudo diffusion coefficient; f, perfusion fraction; MTRasym (3.5 ppm), magnetization transfer ratio asymmetry at 3.5 ppm; SUVmax, maximum standardized uptake value; MTV, metabolic tumor volume; TLG, total lesion glycolysis.

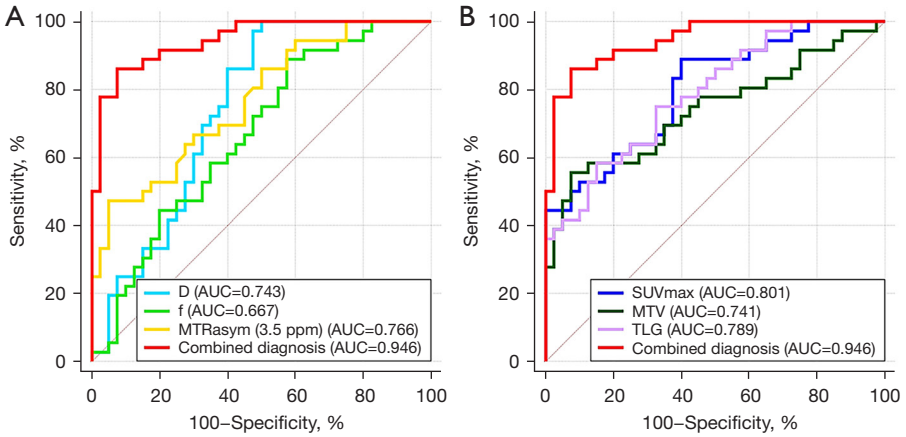

Figure 3 ROC curves of different parameters. (A) ROC curves of D, f, MTRasym (3.5 ppm), and the combination of independent predictors. (B) ROC curves of SUVmax, MTV, TLG, and the combination of independent predictors. D, diffusion coefficient; f, perfusion fraction; MTRasym (3.5 ppm), magnetization transfer ratio asymmetry at 3.5 ppm; AUC, the area under the ROC curve; ROC, receiver operating characteristic; SUVmax, maximum standardized uptake value; MTV, metabolic tumor volume; TLG, total lesion glycolysis.

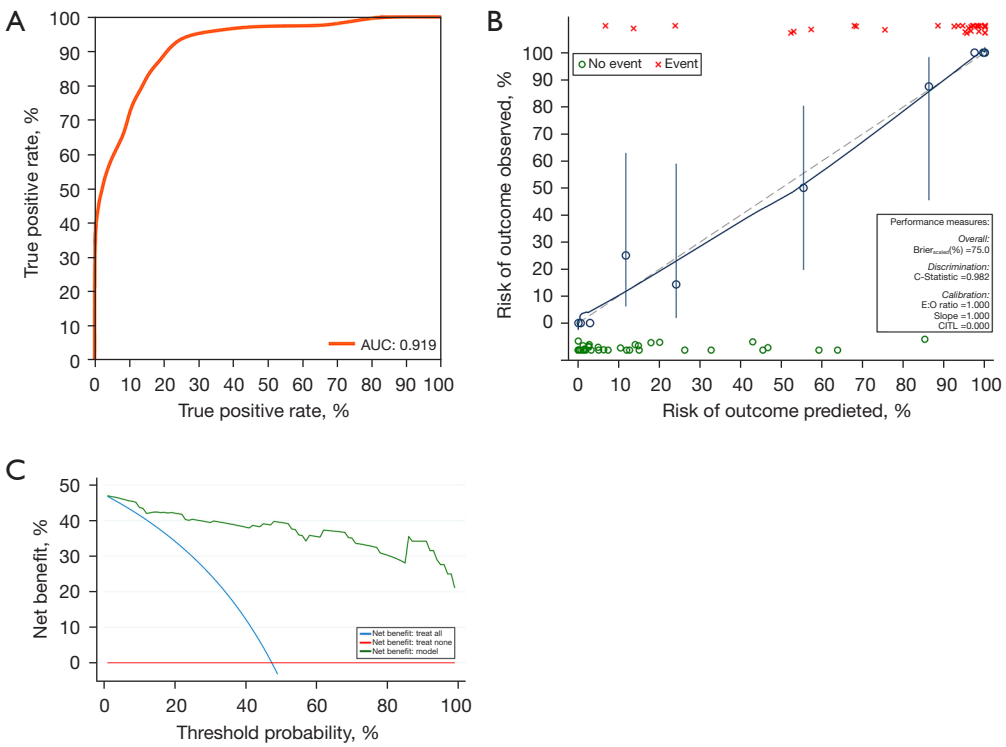

Figure 4 Different curves for predicting PD-L1 expression status in the validation model. (A) ROC curves, (B) calibration curves, and (C) decision curve analysis. AUC, the area under the ROC curve; E:O, expected value: forecast value; CITL, intercept distance; PD-L1, programmed cell death-ligand; ROC, receiver operating characteristic.

is closely related to glucose metabolism (Glut1) and hypoxia (HIF-1α) (11,26). Previous studies have found that NSCLC patients with higher levels of PD-L1 expression usually contain more Glut1 and HIF-1α, so the uptake of ^{18}F-FDG is greater (11,25,26). In the present study, SUV_{max}, MTV, and TLG, three indicators used to reflect ^{18}F-FDG accumulation, were significantly increased in PD-L1-positive NSCLC patients compared with PD-L1-negative NSCLC patients, which is consistent with the above findings and further corroborates the value of metabolic parameters in the noninvasive prediction of PD-L1 expression. However, in multivariate regression analysis, only SUV_{max} was an independent predictor of PD-L1 expression among the three parameters, and several studies also have shown that MTV and TLG are not useful in the assessment of PD-L1 expression (10,27). We speculate that this may be related to the spatial heterogeneity of PD-L1 expression within the tumor (14), which is difficult to accurately characterize by MTV and TLG, reflecting the overall metabolic burden of the lesion. In addition, the different thresholds selected for the calculation of MTV and TLG in different studies may also be one of the reasons for the controversial diagnostic reliability (23).

DWI is the most commonly used quantitative MRI sequence in clinical practice, and the magnitude of its parameter ADC reflects the degree of the restricted diffusion movement of water molecules in tissues (12). There is increasing evidence that different ADC values can not only reflect the tumor microstructure but also predict the expression of biological indicators such as Ki-67, EGFR mutation, and Bcl-2 (14,28). In terms of the prediction of PD-L1 expression, to the best of our knowledge, only a few studies have conducted relevant explorations in head and neck squamous cell carcinomas, and the results showed that there was a weak negative correlation between ADC and PD-L1 expression due to the relatively active metabolism and proliferation of PD-L1-positive cells (13,14). However, the differences in ADC values between the PD-L1-positive and PD-L1-negative groups of NSCLC in this study were not statistically significant, and we speculate that, in addition to differences in tumor types, the rich microcirculatory perfusion of lung cancer may have contributed to this result. Unlike ADC, D in this research was not only able to discriminate between the PD-L1-positive and PD-L1-negative groups of NSCLC but was also one of its independent predictors. This may be because D removes the bias caused by microcirculatory perfusion and thus has the ability to more accurately reflect the diffusion movement of water molecules, providing a better differential diagnosis and higher specificity (15). Yuan *et al.* compared the values of ADC and D in assessing EGFR expression in lung adenocarcinoma and showed that the latter had higher diagnostic efficacy than the former (20). This result supports the above inference to some extent, suggesting that information on the diffusion of water molecules, which is not affected by microperfusion, may more accurately reflect the relevant microenvironmental changes in lung cancer.

Blood perfusion information can also reflect PD-L1 expression to some extent. Meyer *et al.* and Tekiki *et al.* used dynamic contrast-enhanced MRI for the evaluation of head and neck and oral squamous cell carcinomas, respectively, and the results showed that with the increase in PD-L1 expression, the blood perfusion level showed an increasing trend (29,30). The f value is one of the parameters used by IVIM to reflect microcirculatory perfusion, whose magnitude is mainly related to the density of microvessels within the target area (15,31). Kang *et al.* showed that pancreatic cancers with a lack of blood supply had significantly lower f values than normal pancreatic tissue (32), and Shi *et al.* also found a significant decrease in the f value with the application of antiangiogenic factors in NSCLC (33). However, more studies related to lung tumors have shown the opposite result; that is, lung lesions with higher malignancy and a richer blood supply tend to have lower f values instead (31,34), which is generally consistent with the results of the present study. One possible explanation is that the presence of T2 contribution and relaxation effects have an effect on the f value (35). In addition, the complex luminal structure of the lung may also influence the f value to some extent, but this still needs further investigation (31). D* is another perfusion-related parameter of IVIM that is mainly related to blood flow velocity (15). Currently, most studies have found that the reproducibility of D* measurement is poor due to pulsation artifacts from the heart or great vessels, so it is difficult to assess pulmonary lesions effectively (31,34). In this study, there was no significant difference in D* between the PD-L1-negative and PD-L1-positive NSCLC groups, which is generally consistent with the above findings, indicating that the value of D* still needs to be further explored. In addition, some recent studies have suggested that the existing IVIM technique still has limitations in separating perfusion and diffusion component and that this limitation cannot be addressed by high signal-to-noise images, or by an extensive array of b-value images, which may also

contribute to the above results (36-38).

As a relatively novel MRI molecular imaging method, APTWI presents semiquantitative amide proton maps describing the heterogeneous metabolism of mobile proteins and peptides that can reflect the histopathological and genetic changes in tumors (16,17,39). Previous work has shown that higher APTWI signals indicate a high level of mobile protein and peptide metabolism, which was associated with more active cell proliferation, more microscopic necrosis (40), greater microvascular density (41), and an appropriate pH level (42). In the present investigation, compared to NSCLC patients who were PD-L1 negative, NSCLC patients who were PD-L1 positive had higher MTRasym (3.5 ppm) values, most likely due to active tumor cell proliferation (13,14), more necrosis (10), and higher microvascular density (29,30).

A control model with 1,000 bootstrapped samples was built to check the reliability of the multi-factor model, which means that 1,000 samples were randomly selected at the original data and one was chosen as the data result of the control model (43). This was repeated 70 times (the number of patients in the original model), resulting in a control model. The control model yielded the same findings [the combination of SUV_{max}, MTRasym (3.5 ppm), and D] with good accuracy (AUC =0.919) and consistency.

Several limitations of this research should be taken into account. First, this was a single-center study, and the sample size was relatively small, which may have contributed to selection bias. Second, the expression level of PD-L1 may vary depending on the PD-L1 antibody clone (44), and in this study, only a single antibody was used for the immunohistochemistry of PD-L1, which may have some influence on the experimental results. Third, respiratory motion and cardiac and macrovascular pulsations are evident in the chest, and despite the use of respiratory navigation techniques in this study, the display of the lesion was still affected by the cardiac and macrovascular pulsations artifacts, which may cause inaccuracies in some of the MRI-related parameters, especially IVIM and APTWI. Finally, The APTWI sequence used in this study is two-dimensional, and although we copy the position, layer thickness, and layer spacing of the previous sequence layer by layer during the scanning process, this may still introduce errors. Currently, 3D scanning of APTWI has been reported (45), and in the future, we will refine the related technology and conduct further research.

In conclusion, multiparametric ^{18}F-FDG PET/MRI is beneficial for the noninvasive assessment of PD-L1 expression status in NSCLC patients, and the combination of SUV_{max}, D, and MTRasym (3.5 ppm) may serve as a prognostic biomarker to guide immunotherapy.

Acknowledgments

Funding: This work was supported by the National Key R&D Program of China (No. 2017YFE0103600), the National Natural Science Foundation of China (Nos. 81720108021, 31470047), the Zhongyuan Thousand Talents Plan Project - Basic Research Leader Talent (No. ZYQR201810117), the Zhengzhou Collaborative Innovation Major Project (No. 20XTZX05015), and the Key Project of Henan Province Medical Science and Technology Project (Nos. LHGJ20210001, LHGJ20210005 and LHGJ20190602), and the Henan Provincial Science and Technology Research Projects (Nos. 212102310689, 222102310675).

Footnote

Reporting Checklist: The authors have completed the STARD reporting checklist. Available at https://qims.amegroups.com/article/view/10.21037/qims-22-189/rc

Conflicts of Interest: All authors have completed the ICMJE uniform disclosure form (available at https://qims.amegroups.com/article/view/10.21037/qims-22-189/coif). JY, YY, HL, and ZW report that they are from a commercial company, United Imaging Healthcare (UIH), were MR collaborating scientists providing technical support under the UIH collaboration regulations and had no financial or other conflicts with respect to this study. The other authors have no conflicts of interest to declare.

Ethical Statement: The authors are accountable for all aspects of the work in ensuring that questions related to the accuracy or integrity of any part of the work are appropriately investigated and resolved. The study was conducted in accordance with the Declaration of Helsinki (as revised in 2013). This prospective study was complied with ethical committee standards and approved by the ethics committee of the Zhengzhou University People's Hospital & Henan Provincial People's Hospital (No. 2018067) and informed consent was taken from all individual participants.

References

1. Siegel RL, Miller KD, Jemal A. Cancer statistics, 2020. CA Cancer J Clin 2020;70:7-30.
2. Didkowska J, Wojciechowska U, Mańczuk M, Łobaszewski J. Lung cancer epidemiology: contemporary and future challenges worldwide. Ann Transl Med 2016;4:150.
3. Herbst RS, Soria JC, Kowanetz M, Fine GD, Hamid O, Gordon MS, et al. Predictive correlates of response to the anti-PD-L1 antibody MPDL3280A in cancer patients. Nature 2014;515:563-7.
4. Borghaei H, Paz-Ares L, Horn L, Spigel DR, Steins M, Ready NE, et al. Nivolumab versus Docetaxel in Advanced Nonsquamous Non-Small-Cell Lung Cancer. N Engl J Med 2015;373:1627-39.
5. Brahmer J, Reckamp KL, Baas P, Crinò L, Eberhardt WE, Poddubskaya E, et al. Nivolumab versus Docetaxel in Advanced Squamous-Cell Non-Small-Cell Lung Cancer. N Engl J Med 2015;373:123-35.
6. Fehrenbacher L, Spira A, Ballinger M, Kowanetz M, Vansteenkiste J, Mazieres J, Park K, Smith D, Artal-Cortes A, Lewanski C, Braiteh F, Waterkamp D, He P, Zou W, Chen DS, Yi J, Sandler A, Rittmeyer A; POPLAR Study Group. Atezolizumab versus docetaxel for patients with previously treated non-small-cell lung cancer (POPLAR): a multicentre, open-label, phase 2 randomised controlled trial. Lancet 2016;387:1837-46.
7. Yu H, Boyle TA, Zhou C, Rimm DL, Hirsch FR. PD-L1 Expression in Lung Cancer. J Thorac Oncol 2016;11:964-75.
8. Mu W, Jiang L, Shi Y, Tunali I, Gray JE, Katsoulakis E, Tian J, Gillies RJ, Schabath MB. Non-invasive measurement of PD-L1 status and prediction of immunotherapy response using deep learning of PET/CT images. J Immunother Cancer 2021;9:e002118.
9. Lv Z, Fan J, Xu J, Wu F, Huang Q, Guo M, Liao T, Liu S, Lan X, Liao S, Geng W, Jin Y. Value of 18F-FDG PET/CT for predicting EGFR mutations and positive ALK expression in patients with non-small cell lung cancer: a retrospective analysis of 849 Chinese patients. Eur J Nucl Med Mol Imaging 2018;45:735-50.
10. Jreige M, Letovanec I, Chaba K, Renaud S, Rusakiewicz S, Cristina V, Peters S, Krueger T, de Leval L, Kandalaft LE, Nicod-Lalonde M, Romero P, Prior JO, Coukos G, Schaefer N. 18F-FDG PET metabolic-to-morphological volume ratio predicts PD-L1 tumour expression and response to PD-1 blockade in non-small-cell lung cancer. Eur J Nucl Med Mol Imaging 2019;46:1859-68.
11. Kaira K, Shimizu K, Kitahara S, Yajima T, Atsumi J, Kosaka T, Ohtaki Y, Higuchi T, Oyama T, Asao T, Mogi A. 2-Deoxy-2-fluorine-18 fluoro-d-glucose uptake on positron emission tomography is associated with programmed death ligand-1 expression in patients with pulmonary adenocarcinoma. Eur J Cancer 2018;101:181-90.
12. Usuda K, Ishikawa M, Iwai S, Iijima Y, Motono N, Matoba M, Doai M, Hirata K, Uramoto H. Combination Assessment of Diffusion-Weighted Imaging and T2-Weighted Imaging Is Acceptable for the Differential Diagnosis of Lung Cancer from Benign Pulmonary Nodules and Masses. Cancers (Basel) 2021;13:1551.
13. Meyer HJ, Höhn AK, Surov A. Relationships between apparent diffusion coefficient (ADC) histogram analysis parameters and PD-L 1-expression in head and neck squamous cell carcinomas: a preliminary study. Radiol Oncol 2021;55:150-7.
14. Rasmussen JH, Olin A, Lelkaitis G, Hansen AE, Andersen FL, Johannesen HH, Kjær A, Vogelius IR, Specht L, Bentzen SM, Wessel I, von Buchwald C, Fischer BM. Does multiparametric imaging with 18F-FDG-PET/MRI capture spatial variation in immunohistochemical cancer biomarkers in head and neck squamous cell carcinoma? Br J Cancer 2020;123:46-53.
15. Le Bihan D, Breton E, Lallemand D, Aubin ML, Vignaud J, Laval-Jeantet M. Separation of diffusion and perfusion in intravoxel incoherent motion MR imaging. Radiology 1988;168:497-505.
16. Zhou J, Payen JF, Wilson DA, Traystman RJ, van Zijl PC. Using the amide proton signals of intracellular proteins and peptides to detect pH effects in MRI. Nat Med 2003;9:1085-90.
17. Ohno Y, Yui M, Koyama H, Yoshikawa T, Seki S, Ueno Y, Miyazaki M, Ouyang C, Sugimura K. Chemical Exchange Saturation Transfer MR Imaging: Preliminary Results for Differentiation of Malignant and Benign Thoracic Lesions. Radiology 2016;279:578-89.
18. Ohno Y, Kishida Y, Seki S, Yui M, Miyazaki M, Koyama H, Yoshikawa T. Amide proton transfer-weighted imaging

to differentiate malignant from benign pulmonary lesions: Comparison with diffusion-weighted imaging and FDG-PET/CT. J Magn Reson Imaging 2018;47:1013-21.
19. Zheng Y, Huang W, Zhang X, Lu C, Fu C, Li S, Lin G. A Noninvasive Assessment of Tumor Proliferation in Lung cancer Patients using Intravoxel Incoherent Motion Magnetic Resonance Imaging. J Cancer 2021;12:190-7.
20. Yuan M, Pu XH, Xu XQ, Zhang YD, Zhong Y, Li H, Wu JF, Yu TF. Lung adenocarcinoma: Assessment of epidermal growth factor receptor mutation status based on extended models of diffusion-weighted image. J Magn Reson Imaging 2017;46:281-9.
21. Chen S, Gu Y, Yu H, Chen X, Cao T, Hu L, Shi H. NEMA NU2-2012 performance measurements of the United Imaging uPMR790: an integrated PET/MR system. Eur J Nucl Med Mol Imaging 2021;48:1726-35.
22. Liu G, Cao T, Hu L, Zheng J, Pang L, Hu P, Gu Y, Shi H. Validation of MR-Based Attenuation Correction of a Newly Released Whole-Body Simultaneous PET/MR System. Biomed Res Int 2019;2019:8213215.
23. Foster B, Bagci U, Mansoor A, Xu Z, Mollura DJ. A review on segmentation of positron emission tomography images. Comput Biol Med 2014;50:76-96.
24. Kaira K, Higuchi T, Naruse I, Arisaka Y, Tokue A, Altan B, Suda S, Mogi A, Shimizu K, Sunaga N, Hisada T, Kitano S, Obinata H, Yokobori T, Mori K, Nishiyama M, Tsushima Y, Asao T. Metabolic activity by 18F-FDG-PET/CT is predictive of early response after nivolumab in previously treated NSCLC. Eur J Nucl Med Mol Imaging 2018;45:56-66.
25. Seol HY, Kim YS, Kim SJ. Predictive value of 18F-fluorodeoxyglucose positron emission tomography/computed tomography for PD-L1 expression in non-small cell lung cancer: A systematic review and meta-analysis. Thorac Cancer 2020;11:3260-8.
26. Lopci E, Toschi L, Grizzi F, Rahal D, Olivari L, Castino GF, Marchetti S, Cortese N, Qehajaj D, Pistillo D, Alloisio M, Roncalli M, Allavena P, Santoro A, Marchesi F, Chiti A. Correlation of metabolic information on FDG-PET with tissue expression of immune markers in patients with non-small cell lung cancer (NSCLC) who are candidates for upfront surgery. Eur J Nucl Med Mol Imaging 2016;43:1954-61.
27. Cui Y, Li X, Du B, Diao Y, Li Y. PD-L1 in Lung Adenocarcinoma: Insights into the Role of 18F-FDG PET/CT. Cancer Manag Res 2020;12:6385-95.
28. Shieh G. Choosing the best index for the average score intraclass correlation coefficient. Behav Res Methods 2016;48:994-1003.
29. Meyer HJ, Höhn AK, Surov A. Associations between histogram analysis parameters derived from dynamic-contrast enhanced MRI and PD L1-expression in head and neck squamous cell carcinomas. A preliminary study. Magn Reson Imaging 2020;72:117-21.
30. Tekiki N, Fujita M, Okui T, Kawai H, Oo MW, Kawazu T, Hisatomi M, Okada S, Takeshita Y, Barham M, Nagatsuka H, Yanagi Y, Asaumi JI. Dynamic contrast-enhanced MRI as a predictor of programmed death ligand-1 expression in patients with oral squamous cell carcinoma. Oncol Lett 2021;22:778.
31. Wang LL, Lin J, Liu K, Chen CZ, Liu H, Lv P, Fu CX, Zeng MS. Intravoxel incoherent motion diffusion-weighted MR imaging in differentiation of lung cancer from obstructive lung consolidation: comparison and correlation with pharmacokinetic analysis from dynamic contrast-enhanced MR imaging. Eur Radiol 2014;24:1914-22.
32. Kang KM, Lee JM, Yoon JH, Kiefer B, Han JK, Choi BI. Intravoxel incoherent motion diffusion-weighted MR imaging for characterization of focal pancreatic lesions. Radiology 2014;270:444-53.
33. Shi C, Liu D, Xiao Z, Zhang D, Liu G, Liu G, Chen H, Luo L. Monitoring Tumor Response to Antivascular Therapy Using Non-Contrast Intravoxel Incoherent Motion Diffusion-Weighted MRI. Cancer Res 2017;77:3491-501.
34. Liang J, Li J, Li Z, Meng T, Chen J, Ma W, Chen S, Li X, Wu Y, He N. Differentiating the lung lesions using Intravoxel incoherent motion diffusion-weighted imaging: a meta-analysis. BMC Cancer 2020;20:799.
35. Sumi M, Van Cauteren M, Sumi T, Obara M, Ichikawa Y, Nakamura T. Salivary gland tumors: use of intravoxel incoherent motion MR imaging for assessment of diffusion and perfusion for the differentiation of benign from malignant tumors. Radiology 2012;263:770-7.
36. Wáng YXJ. Mutual constraining of slow component and fast component measures: some observations in liver IVIM imaging. Quant Imaging Med Surg 2021;11:2879-87.
37. Wáng YXJ. A reduction of perfusion can lead to an artificial elevation of slow diffusion measure: examples in acute brain ischemia MRI intravoxel incoherent motion studies. Ann Transl Med 2021;9:895.
38. Wáng YXJ. Observed paradoxical perfusion fraction elevation in steatotic liver: An example of intravoxel incoherent motion modeling of the perfusion component constrained by the diffusion component. NMR Biomed

2021;34:e4488.
39. Zhuo Z, Qu L, Zhang P, Duan Y, Cheng D, Xu X, Sun T, Ding J, Xie C, Liu X, Haller S, Barkhof F, Zhang L, Liu Y. Prediction of H3K27M-mutant brainstem glioma by amide proton transfer-weighted imaging and its derived radiomics. Eur J Nucl Med Mol Imaging 2021;48:4426-36.
40. Chen Y, Wang X, Su T, Xu Z, Wang Y, Zhang Z, Xue H, Zhuo Z, Zhu Y, Jin Z, Zhang T. Feasibility evaluation of amide proton transfer-weighted imaging in the parotid glands: a strategy to recognize artifacts and measure APT value. Quant Imaging Med Surg 2021;11:2279-91.
41. Zheng S, van der Bom IM, Zu Z, Lin G, Zhao Y, Gounis MJ. Chemical exchange saturation transfer effect in blood. Magn Reson Med 2014;71:1082-92.
42. Ray KJ, Simard MA, Larkin JR, Coates J, Kinchesh P, Smart SC, Higgins GS, Chappell MA, Sibson NR. Tumor pH and Protein Concentration Contribute to the Signal of Amide Proton Transfer Magnetic Resonance Imaging. Cancer Res 2019;79:1343-52.
43. Xu C, Yu Y, Li X, Sun H. Value of integrated PET-IVIM MRI in predicting lymphovascular space invasion in cervical cancer without lymphatic metastasis. Eur J Nucl Med Mol Imaging 2021;48:2990-3000.
44. McLaughlin J, Han G, Schalper KA, Carvajal-Hausdorf D, Pelekanou V, Rehman J, Velcheti V, Herbst R, LoRusso P, Rimm DL. Quantitative Assessment of the Heterogeneity of PD-L1 Expression in Non-Small-Cell Lung Cancer. JAMA Oncol 2016;2:46-54.
45. Sartoretti E, Sartoretti T, Wyss M, Reischauer C, van Smoorenburg L, Binkert CA, Sartoretti-Schefer S, Mannil M. Amide proton transfer weighted (APTw) imaging based radiomics allows for the differentiation of gliomas from metastases. Sci Rep 2021;11:5506.

Cite this article as: Meng N, Fu F, Sun J, Feng P, Luo Y, Wu Y, Li X, Yuan J, Yang Y, Liu H, Wang Z, Wang M. Sensitivity and specificity of amide proton transfer-weighted imaging for assessing programmed death-ligand 1 status in non-small cell lung cancer: a comparative study with intravoxel incoherent motion and ^{18}F-FDG PET. Quant Imaging Med Surg 2022;12(9):4474-4487. doi: 10.21037/qims-22-189

